Atmos. Meas. Tech. Discuss., 6, 2183–2225, 2013
www.atmos-meas-tech-discuss.net/6/2183/2013/
doi:10.5194/amtd-6-2183-2013

Atmospheric Measurement Techniques
Discussions
Open Access

An automated setup to measure paleoatmospheric $\delta^{13}C-CH_4$, $\delta^{15}N-N_2O$ and $\delta^{18}O-N_2O$ in one ice core sample

P. Sperlich[1,*], **C. Buizert**[1,**], **T. M. Jenk**[1,***], **C. J. Sapart**[2], **M. Prokopiou**[2],
T. Röckmann[2], **and T. Blunier**[1]

[1]Centre for Ice and Climate (CIC), Niels Bohr Institute, University of Copenhagen, Denmark
[2]Institute for Marine and Atmospheric Research in Utrecht (IMAU), University of Utrecht, the Netherlands
[*]now at: Max-Planck-Institute for Biogeochemistry (MPI-BGC), Jena, Germany
[**]now at: Oregon State University, Corvallis, USA
[***]now at: Paul Scherrer Institute, Villigen, Switzerland

Received: 27 January 2013 – Accepted: 18 February 2013 – Published: 28 February 2013

Correspondence to: P. Sperlich (sperlich@nbi.ku.dk)

Published by Copernicus Publications on behalf of the European Geosciences Union.

Abstract

Air bubbles in ice core samples represent the only opportunity to study the isotopic variability of paleoatmospheric CH_4 and N_2O. The highest possible precision in isotope measurements is required to maximize the resolving power for CH_4 and N_2O sink and source reconstructions. We present a new setup to measure $\delta^{13}C-CH_4$, $\delta^{15}N-N_2O$ and $\delta^{18}O-N_2O$ isotope ratios in one ice core sample, with a precision of 0.09 ‰, 0.6 ‰ and 0.7 ‰, respectively, as determined on 0.6–1.6 nmol CH_4 and 0.25–0.6 nmol N_2O. The isotope ratios are referenced to the VPDB scale ($\delta^{13}C-CH_4$), the N_2-air scale ($\delta^{15}N-N_2O$) and the VSMOW scale ($\delta^{18}O-N_2O$). Ice core samples of 200–500 g are melted while the air is constantly extracted to minimize gas dissolution. A helium carrier gas flow transports the sample through the analytical system. A gold catalyst is used to oxidize CO to CO_2 in the air sample without affecting the CH_4 and N_2O sample. CH_4 and N_2O are then separated from N_2, O_2, Ar and CO_2 before they get pre-concentrated and separated by gas chromatography. While the separated N_2O sample is immediately analysed in the mass spectrometer, a combustion unit is required for $\delta^{13}C-CH_4$ analysis, which is equipped with a constant oxygen supply as well as a post-combustion trap and a post-combustion GC-column (GC-C-GC-IRMS). The post combustion trap and the second GC column in the GC-C-GC-IRMS combination increase the time for $\delta^{13}C-CH_4$ analysis which is used to measure $\delta^{15}N-N_2O$ and $\delta^{18}O-N_2O$ first and then $\delta^{13}C-CH_4$. The analytical time is adjusted to ensure stable conditions in the ion-source before each sample gas enters the IRMS, thereby improving the precision achieved for measurements of CH_4 and N_2O on the same IRMS. After the extraction of the air from the ice core sample, the analysis of CH_4 and N_2O takes 42 min. The setup is calibrated by analyzing multiple isotope reference gases that were injected over bubble-free-ice samples. We show a comparison of ice core sample measurements for $\delta^{13}C-CH_4$ that are of excellent reproducibility and accuracy, and in good agreement with previously published data.

1 Introduction

Methane (CH_4) and nitrous oxide (N_2O) are important long-lived greenhouse gases that play a significant role in Earth's radiative budget. The analyses of ancient air as archived in air bubbles within the polar ice sheets significantly improved the understanding of Earth's atmospheric variability. In general, periods of warmer climate in the Northern Hemisphere correlated with increased concentrations of CH_4 and N_2O in the atmosphere (Flückiger et al., 2004; Loulergue et al., 2008; Schilt et al., 2010). The present atmospheric mixing ratios of CH_4 and N_2O are 1774 and 319 ppb respectively (Solomon et al., 2007). They have significantly increased since pre-industrial times, largely due to human activities (Solomon et al., 2007). With the prospect of continuously increasing mixing ratios of CH_4 and N_2O and their impact on future climate, it is important to thoroughly understand the biogeochemical processes related to both gases.

Brenninkmeijer et al. (2003) describe how the isotope fractionation of specific source and sink processes affect the aggregated isotopic composition of the respective trace gases in the atmosphere. In an inverse approach, ice core isotope records of CH_4 and N_2O provide distinct constraints on biogeochemical processes that can be linked to the variability observed in the CH_4 and N_2O mixing ratios on decadal to millennial time scales (Sowers et al., 2003, 2005; Sowers, 2006, 2009; Ferretti et al., 2005; Schaefer et al., 2006; Fischer et al., 2008; Bock et al., 2010b; Melton et al., 2012; Sapart et al., 2012b). Because ice core records of CH_4 and N_2O isotopic composition indicate the natural response of specific greenhouse gas sinks and sources to paleoclimate changes, this information is of great interest to global warming predictions.

Here, we present a method to simultaneously measure $\delta^{13}C$ isotope ratios of CH_4 as well as $\delta^{15}N$ and $\delta^{18}O$ isotope ratios of N_2O in a single ice core, firn gas or atmospheric sample By melting ice core samples under vacuum, between 20 and 50 mL of air can be extracted from 200–500 g of ice for isotopic analysis. Alternatively, atmospheric samples and isotope reference gases can be injected into the system. The system is highly automated and comprises of custom made units to separate CH_4 and N_2O from the main air components (N_2, O_2, Ar) and other trace gases (CO_2, CO) before using a modified gas-chromatography combustion unit coupled to a single isotope ratio mass spectrometer in continuous flow mode for isotope ratio determination. The combustion unit converts CH_4 to CO_2 so that the $\delta^{13}C-CH_4$ is measured as $\delta^{13}C\text{-}CO_2$ on the triple collector system of a mass spectrometer (Merritt et al., 1995). We introduced a scheme of permanent oxidation with a post-combustion cryo-trap, followed by a second GC column, similar to (Melton et al., 2011). This method ensures a stable oxidation of the combustion reactor with minimized oxygen load into the IRMS and it excludes interferences of the $\delta^{13}C-CH_4$ measurement with Kr inside the IRMS (Schmitt et al., 2013). The system is anchored to the international isotope scales using isotope reference gases that were synthesized after Sperlich et al. (2012) for $\delta^{13}C-CH_4$ or calibrated by intercomparison measurements with an external laboratory for $\delta^{15}N-N_2O$ and $\delta^{18}O-N_2O$. A novelty of this system is the automated sample preparation to measure isotope ratios of two isobaric gas species from one ice core sample using one mass spectrometer in an online measurement mode. Furthermore, we introduce a catalyst for quantitative oxidation of CO which – to our knowledge – has hitherto not been used in setups for atmospheric measurements. We suggest the presented system as a useful tool for the isotopic analysis of paleoatmospheric CH_4 and N_2O to provide high precision data that are important for current climate research.

2 Experimental setup

2.1 Extraction system

The extraction unit (Fig. 1) represents the interface for sample and isotope reference gas introduction into the analytical setup and it includes the first step to separate the analytes from the main air components (N_2, O_2 and Ar). The sample lines of the extraction system are made of 1/4″ stainless steel (SST) tubes and Swagelok components

(Swagelok, USA) except for the two six-port valves (V1 and V2) that are manufactured by VICI (VICI, USA) and connected to 1/16″ SST tubing. All connections are either welded or sealed with metal gaskets to exclude artefacts due to out-gassing of polymer gaskets (Sturm et al., 2004). All analytical lines are either continuously flushed by a helium gas stream (99.9995 % helium, Air Liquide, Denmark) or permanently under vacuum.

The gas-manifold enables the injection of gas from up to four different gas tanks or sample flasks into the extraction unit via a mass flow controller (referred to as MFC, manufactured by MKS, model 1179A, specified for N_2, 200 mL min^{-1}). A 100 mL sample volume parallel to the MFC can be used to take aliquots by expansion of gases from the gas manifold into the volume. A pressure gauge ("P1", Keller, 21Y, max. 2 bar) is then used to calculate the amount of air in the sample volume. However, in regular practice, the good performance of the computer controlled MFC replaced the manual injection method through the sample volume. We use two principle methods to introduce samples:

(i) Ice core samples can be introduced into the 1.25 L melt-vessel in which the ice sample is melted (SST-glass adapter, DN 100, MDC vacuum, UK). Isotope reference gases or air from flask samples can also be introduced into the melt-vessel or into the water trap (T1) using manual valves and either the MFC or the sample volume. T1 comprises of 20 cm DN 50 SST tube that is welded to a quick flange connector and sealed with an aluminium gasket. Both 1/4″ tubes connecting the water trap are welded onto the opposing quick flange cap. The water trap is filled with glass beads of 3 mm diameter that make a minimum path length through the glass beads of ≥ 50 mm. T1 is cooled with a dry-ice/ethanol bath to −78 °C. The second pressure gauge ("P2", Edwards APG100-LC, minimum pressure 10^{-4} mbar) is mounted between T1 and the air-extraction trap (T2) to monitor vacuum and extraction efficiency. T2 contains 1.5 g Hayesep-D (60/80 mesh, Sigma-Aldrich) which adsorbs the gas sample from the extraction line when the trap is cooled to liquid nitrogen (LN_2) temperature. Intensive extraction tests using several charcoal adsorbents in T2 showed additional

CH_4 contribution and a high variability in isotopic analysis in our setup. We found that the speed of adsorption can significantly be increased with larger cross-sections of the adsorbing trap. Therefore, T2 is built from a SST housing (ID ~ 15 mm, F-type filter, Swagelok) welded to a U-shaped 1/4″ SST tube. The Hayesep-D is held in place by glass-wool and a double-layered SST mesh of concave shape, thereby doubling the effective surface of the SST mesh. T2 adsorbs about 200 mL air from the extraction line in less than 15 min. The trap is equipped with a PID-controlled (Proportional-Integral-Derivative) heating wire (4 m, 12.5 Ohm m-1, Type 1 NC 1, Thermocoax) that heats the trap to the desorption temperature of 50 °C in less than 1 min when an automated lift removes the LN_2 dewar from T2. The air sample is then transported by the extraction flow of 50 $mL\,min^{-1}$ helium. A capillary above T2 maintains a 2 $mL\,min^{-1}$ helium flush-flow in the lines connecting T2 when the valves of T2 towards V1 are closed (Fig. 1). The SST line and the valves that connect melt-vessel with T1 and T2 are thermally insulated and constantly held at 55 °C with a PID controlled heating wire to increase the water vapour pressure so any ice core sample derived water can be more efficiently trapped in T1.

(ii) Alternatively, the MFC can inject gas from pressurized tanks into the 50 $mL\,min^{-1}$ helium flow directly when V1 and the manual valves are set accordingly (Fig. 1). This option bypasses T2, thereby minimizing the manual valve operation and analysis time.

For both sample introduction methods, the sample gas is transported by the same 50 $mL\,min^{-1}$ helium flow through the CO oxidizer (Aurolite™, Au/TiO_2, Strem Chemicals, described in Sect. 2.7). From there, the sample is routed to a separation trap (T3), which is a modification of the principle described by DesMarais, (1978). A 1/8″ SST tube is filled with Hayesep D (80/100 mesh, Sigma-Aldrich, Switzerland) and precisely temperature-controlled to −153, −122, −10 and 50 °C over a length of 30 cm using a PID-controlled heating wire and a Pt-1000 temperature sensor (the temperature stability is better than ±0.4 °C). A loop of this 1/8″ tube section is routed through a DN 40 SST-cylinder, which can be evacuated or filled with helium. The lower part of the DN 40 cylinder is submerged in LN_2. To cool T3, the heat conductivity between the Hayesep-D filled 1/8″ tube and the DN 40 cylinder cooled by LN_2 is increased by pressurizing the latter with helium to 2.5 bar. When the trap is heated to −10 or 50 °C the DN 40 cylinder is evacuated. T3 retains CH_4, N_2O, CO_2 and Kr at temperatures ≤ -122 °C while N_2, O_2 and Ar pass through. The amount of eluting N_2, O_2 and Ar is measured with a Thermal Conductivity Detector (micro-TCD, VICI) to enable CH_4 and N_2O mixing ratio analysis from the total amount of air analysed and the trace gas peak areas in the IRMS analysis (note that we will not discuss the performance of this mixing ratio determination method as it is by an order of magnitude less precise than conventional GC-systems (Mitchell et al., 2011) or laser analyzers (Stowasser et al., 2012); however, we mention it for its use when more precise mixing ratio data are not available as well as to monitor extraction efficiency and leakages). From T3, the sample is transported through a glass tube of 6 mm outer diameter (OD) and 600 mm length which holds Ascarite™ (NaOH, Sigma Aldrich) and $Mg(ClO_4)_2$ (Merck) to remove H_2O, CO_2 and the CO-derived CO_2. The dimensions of this trap combine a relatively long contact-time between the sample gas and the trapping material due to the column-length with a relatively short time required to quantitatively flush the sample through the glass cavity due to the small inner diameter (the amount of trapping material was sufficient for 6 months).

2.2 GC-C-GC-IRMS

The final purification and analysis of the air samples occurs via a combined GC-C-GC-IRMS setup (Fig. 2) after the ice core and air extraction unit. All valves are two position VICI valves, all tubing either 1/16″ SST tubes or fused silica capillaries. Valve V4 provides the helium flows of 10 mL min^{-1} and 1 mL min^{-1} that are used to transfer the pre-concentrated sample from T3 to T4 and from T4 to the GC column (GC 1), respectively. T4 is a 55 cm section of GC-column (Pora-Bond Q, 0.25 mm ID Agilent) that can be submerged in LN_2 to cryo-focus the target gases. V4 enables to route either the 10 or the 1 mL min^{-1} helium flow through the injector valve V3 (2 µL, VICI) for

~ 1 nmol sized injections of pure CH_4 and N_2O into T3 or T4. These injections were used to tune the timing of the sequences and to monitor the reproducibility and drift during the test-phase of the setup. The 10 mL min^{-1} helium stream flows from V4 to the ice extraction unit and returns to valve V5 of the GC-C-GC-IRMS section (Fig. 2). This helium flow cryo-focuses the purified CH_4 and N_2O samples in T4. V5 then routes the 1 mL min^{-1} helium flow through T4 to introduce the sample gases into GC 1 (Pora-Bond Q, 0.25 mm ID, 25 m length, Agilent). GC 1 is submerged in an ethanol bath at −5 °C to increase the chromatographical separation between CH_4 and N_2O to ~ 160 s. GC 1 can be placed in an oven at 80 ° C for desorption of H_2O during stand-by time. While it is possible to measure $\delta^{15}N$ and $\delta^{18}O$ in N_2O directly using GC-IRMS, CH_4 samples need to be combusted to CO_2 for $\delta^{13}C$ analysis (Merritt et al., 1995). The CH_4 elutes from GC 1 before N_2O and is routed to the combustion unit via V6. The combustion reactor contains 3 Ni wires (99.994 %), 3 Cu wires (99.9999 %) to store and provide oxygen during combustion and 2 Pt wires (99.997 %) to catalyze the combustion, (all wires are 0.1 mm OD, Alfa Aesar, UK). A small flow of oxygen is constantly added to guarantee maximum oxidation of the combustion reactor at all times, which is the relevant parameter for a high CH_4 combustion rate (Cullis and Willatt, 1983). This method yields quantitative combustion of samples that greatly differ in CH_4 amounts such as ice core samples. Water originating from the combustion process is removed by a Nafion membrane (60 cm length, TT-020, Permapure, USA) and a helium counter-flow of 7 mL min^{-1} at −5 °C. The eluting CH_4-derived CO_2 is trapped on T5 comprising of a fused silica capillary (350 µm ID, 55 cm length) submerged in LN_2. To increase the trapping efficiency and to prevent the flaky CO_2 from blow-out the capillary trap T5 contains a nickel wire (99.994 % Ni, 0.1 mm OD, Alfa Aesar), (e.g. Brand, 1995; Behrens et al., 2008). When the CH_4-derived CO_2 is trapped in T5, V6 redirects the GC-flow to analyze the N_2O first. V6 and V7 are then switched and T5 is removed from the LN_2 bath to pass the CH_4-derived CO_2 through GC 2 which is held at 40 °C (Pora-Bond Q, 0.25 mm ID, 25 m length, Agilent) prior to measuring the CH_4-derived CO_2. Helium flushed purge housings are used on valves V3–V6.

2.3 Sample and system preparation

Measurements of ice samples began with cooling of the H_2O trap T1 in a dry-ice ethanol bath. Therefore, T1 was pressurized with helium to ~1500 mbar to increase the heat conduction within the glass bead bed for ~2 h. GC 1 was placed in the ethanol bath at −5 °C if it was previously heated to 80 °C. Meanwhile, ice core samples which were stored at −25 °C were prepared in the cold room at −15 °C. The surface of all sample pieces was cleaned following a decontamination protocol of removing the top 3–5 mm with a band-saw. Afterwards, saw dust attached to of each piece of ice was removed with a scalpel and a brush while the ice sample was carefully checked for anomalous features. Cracked parts were removed from each sample to prevent from contamination by laboratory air and/or drill-fluid intrusion. Also, layers of outstandingly high content of dust or soot particles were cut out. On average, 30 % was removed from each sample. The decontaminated ice sample and a glass-coated magnet stir-bar were then placed inside the melt-vessel, which was sealed with a copper gasket and fastened with 16 bolts to 25 Nm torque. Two samples were prepared and transferred to a chest freezer at −20 °C to be analyzed the same day. The analytical system was finally prepared by evacuating T1 as well as all lines and pressure-regulators of the atmospheric isotope reference gases connected to the gas-manifold (Fig. 1). The measurement routine was started when the pressure inside the extraction system reached 10^{-3} mbar, indicating absence of significant air-leakage and remainders of water from previously analyzed samples.

After every day of ice core measurements, the melt vessel was carefully cleaned with ultra-pure water and a detergent soap for laboratory glassware (Alconox, USA), as suggested by Mitchell et al. (2011). The glassware was thereafter dried at 80 °C over night. To extract the water that was trapped during the ice core measurements, T1 was heated to 150 °C with a PID controlled heating-sleeve and kept under vacuum until it was used next. The water was thus transferred from the extraction line to the water trap near to the vacuum pump. This method prevented from frequent opening of the connectors of the extraction line.

2.4 Measurement routine

2.4.1 Ice core samples

In order to minimize the time between the measurements, samples were introduced into the extraction unit while the previous sample was analyzed in the GC-C-GC-IRMS section of the setup. This resulted in a sample interval of only 42 min. Ice core samples and isotope reference gases were treated as similar as possible, to balance analytical effects during analysis following the principle of identical treatment (Werner and Brand, 2001). However, a difference exists in the application and extraction of ice core and isotope reference gas sample. The MFC was used to inject isotope reference gas into T1 that was extracted from there onto T2. In contrast, ice core samples were introduced into the melt-vessel where they slowly released the air sample which was cryo-pumped through T1 onto T2 during melting. This is the only gas handling difference between ice core sample and isotope reference gas. We tested for isotope fractionation effects based on the different gas handling but found no significant isotope fractionation in our setup as will be explained in Sect. 3.5. The ice core air was continuously extracted from the melt-vessel as the ice was melting, to minimize the pressure and thereby the time the gas was in contact with the melt water to reduce the dissolved gas fraction.

Each analysis began with the evacuation of the extracting unit. The thoroughly cooled T1 represents the cavity for isotope reference gas extractions and was evacuated for 6 min prior to reference gas introduction. To measure an ice core sample, the melt-vessel was attached during the previous isotope reference gas measurement so it could be evacuated for 20–30 min without delaying the measurement routine. During evacuation, the melt-vessel was cooled in an ice water bath to prevent the sample from melting ahead of schedule. Even though laboratory air was sufficiently removed from the melt-vessel after ~5 min evacuation time (in line with Schaefer and Whiticar, 2007), extending the evacuation time helped decontaminating the ice core sample by sublimating the surfaces of the ice sample and evacuating the ice bubbles just below the surface. The measurement routine then continued with cooling T2 in LN_2 for 8 min in preparation for the extraction of ice core air or isotope reference gases. Towards the end of cooling T2, either an isotope reference gas was injected into T1 or the ice bath under the melt-vessel was replaced by a hot water bath (60 °C) to start melting the ice. As T2 cooled for 8 min, the air extraction was started by opening the valve between T1 and T2 and the melt-vessel for ice extractions. After extracting 40 mL of isotope reference gas for 13 min, the pressure within the extraction unit decreased from 14 mbar to 0.07 mbar, indicating 99.5 % extraction efficiency. The pressure development during air extractions was found to be very reproducible and only varied with the amount of air and the variable melting time from ice samples of variable size. By ensuring that both isotope reference gas and all ice core samples were extracted to similar pressures, the principle of identical treatment was met and potential isotope fractionation effects based on variable completeness of extraction cancelled out. The timing was controlled by the IRMS operating software (ISODAT); the ISODAT script was started manually when ice samples were extracted to 0.11 mbar. After the extraction, all standards and samples underwent identical analytical treatment, precisely timed by the ISODAT script. First T3 was cooled to −154 °C within one minute and was held constant by the PID controller. After T3 cooled for 4 min, the extraction was stopped. T2 was heated from −196 °C to 50 °C in less than one minute, thereby releasing the sample within the carrier gas flow of 50 $\mathrm{mL\,min^{-1}}$ helium which transfers the sample from T2 through the CO-oxidizer to T3. T3 separated N_2, O_2 and Ar from the sample gas mixture and retained CH_4, N_2O, CO_2 and Krypton on the Hayesep D. At the same time, the temperature of T3 was increased to −122 °C to improve the separation performance of T3 (Umezawa et al., 2009). The TCD signal to measure the amount of N_2, O_2 and Ar was recorded using a LabView script. The separation in T3 was completed after 400 s. V2 was then switched and T3 heated to −10 °C to transport the trace gases in a helium flow of 10 $\mathrm{mL\,min^{-1}}$ from T3 through the chemical trap onto the capillary trap T4, which was submerged in LN_2 10 s before. CH_4 and N_2O were focussed in T4 after 360 s. V2 was then switched and T3 heated to 50 °C to vent residual water. Next, V5 was switched and the analytical helium flow of 1 mL min^{-1} transported both sample gases from T4 through GC 1 as T4 was lifted from the LN_2 bath. It took the CH_4 about 220 s to pass through GC 1 and to enter the combustion oven. After 200 s, the post-combustion trap T5 was lowered into a LN_2 bath to trap the CH_4-derived CO_2. Using the post combustion-trap strictly requires the elimination of any potential interference of nonCH_4 gases (CO, Kr, CO_2 and N_2O) with the CH_4-derived CO_2 in the mass spectrometer. At −5 °C, CO eluted from GC 1 just before CH_4. To prevent CO from entering the combustion oven and T5 and thereby contaminating the CH_4-derived CO_2, CO was quantitatively eliminated in the CO-oxidizer (Sect. 2.7). Kr eluted from GC 1 at the same time as CH_4 and could interfere with the analysis of CH_4 derived CO_2 unless separated (Schmitt et al., 2013). We show that our $\delta^{13}C-CH_4$ measurements were unaffected by Kr in (Sect. 2.6). The Ascarite trap (Fig. 1) lowered the content of CO_2 by 5–6 orders of magnitude, however, remnant CO_2 was described to pass through (Röckmann et al., 2003). We observed a very small CO_2 remainder (1.5 mV intensity) during the N_2O measurement, that represented CO_2 passing through the Ascarite trap as well as the CO_2 system blank. This peak was well separated from the sample N_2O by 70 s and useful to monitor the exhaustion of the Ascarite trap. The preconcentration in T4 also traps N_2 and O_2 remainders, stemming from incomplete separation in T3. N_2 and O_2 are reported to form traces of N_2O in the combustion oven that isobarically interferes with the CH_4-derived CO_2 in the IRMS (e.g. Vaughn, 2004; Umezawa et al., 2009). With the application of GC 2, we can also exclude any isobaric interference of N_2O artefacts. We therefore conclude that our system is free of any of the interferences discussed above.

After 80 s of post-combustion trapping, all CH_4-derived CO_2 was trapped in T5 and V6 was switched to route the chromatographic flow directly to the open split and the IRMS for the isotopic measurement of N_2O. Meanwhile, V7 was switched to a pure helium flow of 1 mL min^{-1} to remove the oxygen from T5. When the N_2O measurement was completed, V6 was switched and routed the CH_4-derived CO_2 from T5 through GC 2 into the open split for isotopic analysis in the IRMS. In the mean time, T1 and T2 were evacuated in preparation for the following sample.

2.4.2 Air samples

The analysis of air samples was similar to the analysis of ice core samples and differed only in the fully automated introduction of air samples, if the samples were applied from vessels exceeding atmospheric pressure. Pressurized air tanks were connected to the gas manifold where the MFC introduced the samples through V1 into the 50 mL helium flow (Fig. 1). A sample flow time of 90 s was allowed for the sample and helium flows to equilibrate before V2 was switched to direct the sample onto the pre-cooled T3. After this point, the analysis was exactly the same as described in Sect. 2.4.1, however; only one sample was introduced and analyzed at a time. If the air samples were at sub-ambient pressures, they were introduced into T1 through the sample volume to be extracted like the isotope reference gases during ice core measurements.

2.5 Preparation of IRMS for isotopic measurements of two different gases

While only a small fraction of the analyte molecules entering the ion source of an IRMS get ionized and reach the detector, other sample molecules can be subject to unintended physical and chemical interactions with the analytical system itself but also with molecules of other gas species apparent in the analyzer. Potential effects include system memory, adsorption and desorption of gases altering the background levels, ion reactions (Anicich, 1993), reactions enabled by the hot filament and a combination of all (Brand, 2004). Measuring two isobaric gases such as N_2O and CO_2 in the same sample on the same IRMS can reduce the precision significantly if the conditions inside the IRMS vary throughout the measurements (Carter and Barwick, 2011). To increase the stability of our analyzer, we injected a large pulse of pure isotope reference gas into the ion source for one minute before the start of the respective measurement sequence.

The following measurement sequences comprised of 10 or 12 flat-topped peaks of pure CO_2 or N_2O reference gas for CH_4-derived CO_2 and the N_2O measurement, respectively (Fig. 3). This enabled to simultaneously improve and monitor the reproducibility before the sample peak entered the IRMS. The standard deviation of the 3 flat-topped reference gas peaks preceding the sample was 0.029 ‰ for $\delta^{13}C-CO_2$, 0.061 ‰ for $\delta^{15}N-N_2O$ and 0.086 ‰ for $\delta^{18}O-N_2O$, respectively (average of 66 measurement sequences). These values refer to reference gas peak # 8, 9, 10 in the CH_4-derived CO_2 sequence and 9, 10, 12 in the N_2O sequence (peak number 11 in the N_2O sequence is not considered due to the small contribution of CO_2, (Sect. 2.4.1). Measurements of atmospheric and synthetic air mixtures with precisely referenced $\delta^{13}C-CH_4$ (Sperlich et al., 2012) suggest this conditioning method of the IRMS showed no significant η-effect (Brand, 2004) over $\delta^{13}C-CH_4$ range of 5 ‰, reflecting the magnitude of $\delta^{13}C-CH_4$ variability in firn and ice core samples (e.g. Fischer et al., 2008).

2.6 Excluding Krypton interference

Krypton – which is abundant in the atmosphere at ~1 ppm (Aoki and Makide, 2005) – was found to co-elute from the GC column with CH_4 and to interfere with the analysis of CH_4-derived CO_2 (Schmitt et al., 2013). The system described here deployed a post-combustion cryo-trap followed by a second GC column (Fig. 2). This combination ensured cryogenic separation of CH_4-derived CO_2 and Kr in T5 as only fractions of the Kr got trapped in T5 at LN_2 temperature. After the cryogenic separation, GC 2 ensured chromatographical separation of CH_4-derived CO_2 and remaining Kr. To test the Kr impact, the CO_2 gas configuration was modified to monitor the mass triplet *m/z* 43/44/45 during a CH_4 measurement instead of *m/z* 44/45/46 (Fig. 4). This test showed a crippled peak from $^{86}Kr^{++}$ on *m/z* 43 which precedes the $\delta^{13}C-CH_4$ measurement of atmospheric air with baseline separation of 10 s between Kr and the CH_4-derived CO_2 peak on *m/z* 43 (Fig. 4). In this case, the sample peak produced a small signal on m/z 43 as can also be seen for the three reference gas peaks (pure CO_2) at the beginning of both sequences.

In comparison, injections of pure CH_4 via V3 into T4 underwent exactly the same analytical steps in the GC-C-GC-IRMS section, but did not show the crippled $^{86}Kr^{++}$ peak on m/z 43 at all (Fig. 4). This test identified the crippled peak from $^{86}Kr^{++}$ in the air sample and proved that our $\delta^{13}C-CH_4$ measurements were not affected by Kr interferences.

2.7 CO-oxidizer

Because T5 trapped all LN_2 condensable gases that eluted from the combustion oven, the analysis of the trapped gases could not distinguish whether the detected CO_2 was derived from CH_4 or from any other carbon containing precursor gases different from CH_4. To exclude any spurious CO contribution, the CO was quantitatively oxidized to CO_2 and then removed by the Ascarite trap (Fig. 1). Schütze reagent is often used in analytical setups to oxidize CO to CO_2 at room temperatures when the CO is to be analyzed for its isotopic composition of $\delta^{13}C$ and $\delta^{18}O$ (e.g. Brenninkmeijer, 1993). Alternatively, Sofnocat or Hopcalite can be applied as oxidation catalyst (e.g. Kato et al., 1999). However, the CO-oxidation efficiency of both catalysts decreases with increasing moisture content (McPherson et al., 2009). To our awareness, this is the first system described for atmospheric measurements using Aurolite™ as catalyst to oxidize CO to CO_2. The efficiency of Aurolite™ is reported to even improve with increasing moisture content in the sample gas stream (e.g. Date et al., 2002; McPherson et al., 2009), making it particular suitable for CO elimination in air extracted from melted ice core samples. Our CO-oxidizer comprises of 10 cm 1/4″ SST tube holding 5 cm of Aurolite catalyst between two glass wool plugs that are kept in place by SST meshes at both ends. The CO-oxidizer column is held at 60 °C.

To test the system, a synthetic CH_4- and CO_2 free air with a CO mixing ratio of 350 ppb was mixed in the setup described by Sperlich et al. (2012). This air mixture was applied to the system with and without the CO-oxidizer as well as with a trap holding Schütze reagent (iodine-pentoxide, 99.99 %, Sigma-Aldrich) inside a 6 mm OD glass tube over a length of 150 mm. The timing of the GC-C-GC-IRMS system was adjusted to fully combust, trap and analyse the residual CO that eluted from GC 1. Note, the CO that was oxidized in the CO-oxidizer or in the Schütze reagent was chemically trapped on the Ascarite trap (Fig. 1) and therefore not detected. A series of measurements showed no CO-derived CO_2 peak that exceeded the normal blank peak of the measurement sequence for the tests made with Aurolite™ while up to 90 % of the CO passed through the Schütze reagent unoxidized. Our tests suggest that Aurolite™ quantitatively oxidizes CO in atmospheric samples and is significantly more reliable to oxidize CO than Schütze reagent, while it lacks the moisture sensitivity of Sofnocat and Hopcalite. Aurolite can therefore be used to produce CO-free air for gas mixing purposes or to convert CO to CO_2 in an analytical online system when quantitative conversion is required.

3 System performance

3.1 Shot noise

We modified the approach of Merritt et al. (1994) to calculate the shot-noise with respect to the different analytes and the average peak areas of isotope reference gases and samples. We calculated a shot-noise range on the 1σ-level of 0.04–0.05 ‰ for $\delta^{13}C-CH_4$, 0.11–0.17 ‰ for $\delta^{15}N-N_2O$ and 0.15–0.22 ‰ for $\delta^{18}O-N_2O$, respectively. The calculated shot noise ratio may therefore explain between 40–50 % of the measurement uncertainty for $\delta^{13}C-CH_4$ and between 20–29 % and 21–31 % of the uncertainty of the $\delta^{15}N$ and $\delta^{18}O$ measurements of N_2O, respectively. The remaining uncertainty is then based on the variability of the sample preparation. Generally, the shot-noise ratio is larger for N_2O than for CO_2 due to the lower abundances of the rare isotope (1.1 % ^{13}C, 0.36 % ^{15}N and 0.205 % ^{18}O, e.g. Sessions, 2006) and the signal intensity of N_2O as compared to CH_4-induced CO_2, due to lower mixing ratios (e.g. Schilt et al., 2010) and ionization efficiency (Friedli and Siegenthaler, 1988; Ghosh and Brand, 2004).

3.2 Sample recovery of injected air standards

Figure 5 shows the sample recovery as the response of the system to sample size variations between 0.5 and 3.2 nmol CH_4 and 0.3 and 1.1 nmol N_2O. The measurements are based on the extractions of air samples between 20 and 70 mL, respectively (Sect. 3.5). Since the valves to route the MFC-injection of isotope reference gases into the extraction line were manually controlled, a small variability of the applied volume and hence in IRMS peak area of CH_4-induced CO_2 and N_2O could not be avoided. The linear regression of the average IRMS peak area over the injected sample size shows an R^2 of 0.998 and 0.987 for CH_4 and N_2O, respectively. We therefore conclude the extraction unit and the components of the GC-C-GC-IRMS system responded linearly to sample size variability, indicating appropriate system design and timing steps enabling quantitative analysis within the expected sample size range.

3.3 System blank tests

During an ice core measurement campaign, the system blank was determined after the extraction of each ice core sample (Table 2). For this purpose, the valves of the extraction line were closed when the ice-extraction was completed. The sample vessel with the extracted sample was thereby kept under vacuum but it could collect air from potential leakage into the extraction unit. The extraction volume was then extracted for 5 min and processed as a regular sample. Hence, the detected system blank represented an integrated signal of system leakage, contamination within the analytical gas streams but more importantly, ice sample-specific leakage through the melt-vessel gasket as well as sample remnants from incomplete extractions. We compared the IRMS peak areas of each blank test to the IRMS peak areas of the preceding ice core sample for

35 ice core measurements and found blank peak areas with an average size of 1.5 and 3.0 % of the preceding CH_4 and N_2O sample, respectively. The N_2O blank size neither correlated with the CH_4 blanks nor could any anomalous signal be detected on the TCD, precluding leakage from laboratory air. We speculate the higher N_2O blank values resulted from ice core air remnants due to higher solubility as compared to CH_4. In fact, 12 out of 35 blank tests showed a peak area that exceeded 5 % of the peak area of the preceding N_2O sample. The blank tests of the other 23 ice core samples averaged to 1.1 % of the sample peak area. These tests might indicate limitations in the extraction efficiency for N_2O during the melt-extraction as compared to the extraction efficiency of CH_4. Because the isotope ratios of such small peaks are not unambiguously detectable, we did not apply a blank correction to the sample measurements of CH_4 and N_2O.

During the test phase of the setup, we installed a helium flow of 200 mL min^{-1} to strip dissolved gases from the melted ice core sample after the majority of the gases has been extracted as described in (Sect. 2.4.1). Unlike Behrens et al. (2008) and Bock et al. (2010a), we pumped on the extraction line at the downstream-end of T2 to absorb the sample gases on T2 while removing the helium for 5–10 min. Measurements of ice core samples that were extracted with the stripping-method did neither show a significant blank reduction nor a reduced variability of isotopic analysis for CH_4 and N_2O. The stripping technique was thus excluded from the method.

3.4 Referencing of applied isotope reference gases

Four isotope reference gases were applied to the described setup (Table 1). GIS (Glacial Isotope Standard) refers to a synthetic air mixture that was prepared after Sperlich et al. (2012) with additional N_2O. An atmospheric air tank was sampled in the year 2008 at a clean-air site of the NEEM camp in North-West Greenland and is hereafter referred to as NEEM. Furthermore, we used two synthetic air mixtures called AL and NOAA that were provided by Air Liquide (Teknisk Luft, Air Liquide, Denmark) and the National Oceanic and Atmospheric Administration (NOAA, Boulder, USA), respectively.

The isotope ratio of all reference gases were referenced to the VPDB isotope scale for $\delta^{13}C-CH_4$ and to the $\delta^{15}N$ scale of N_2-air and the $\delta^{18}O$-VSMOW scale for N_2O, respectively. We established the isotope scale for N_2O in our isotope reference gases based on NEEM, the isotopic composition of which is extrapolated after Röckmann and Levin (2005). The integrity of our calibration scale for N_2O isotopic composition was tested by intercalibration measurements of NEEM, AL and NOAA by the Institute for Marine and Atmospheric Research in Utrecht (IMAU), The Netherlands (published in Sapart et al., 2011). The isotopic composition of N_2O in GIS was referenced on the setup described in this paper by calibrating against NEEM and AL. The $\delta^{13}C-CH_4$ in NEEM was calibrated by IMAU and the Institute for Climate and Environmental Physics at the University of Bern, Switzerland (Bern), (Jochen Schmitt, personal communication, 2011). GIS was independently referenced for $\delta^{13}C-CH_4$ and shown to be in excellent agreement with the externally calibrated NEEM air (Sperlich et al., 2012). AL was referenced for $\delta^{13}C-CH_4$ on the described setup based on NEEM and GIS, while NOAA was calibrated for $\delta^{13}C-CH_4$ by NEEM only. The mixing ratios of CH_4 and N_2O in GIS, NEEM and AL were measured at the Max-Planck-Institute for Biogeochemistry (Armin Jordan and Bert Steinberg, personal communication, 2012) while NOAA was provided with certificates. GIS was chosen to reference the isotopic composition of CH_4 and N_2O in ice core samples to the international isotope scales due to the similar mixing ratio of CH_4. Air samples with higher CH_4 mixing ratios, such as NOAA, firn-air or atmospheric samples were referenced against NEEM.

3.5 System calibration with bubble free ice measurements

The principle of identical treatment (Werner and Brand, 2001) was inevitably violated in the way that ice core samples and isotope reference gases were introduced into the system and by the process that was necessary to deliberate the air from the ice core sample. Moreover, the quantity of CH_4 and N_2O in the air of glacial or interglacial ice core samples varies by a factor of ~2 for CH_4. The nature of the ice core samples itself therefore limits to what extend the principle of identical treatment can be applied to analytical systems measuring air in ice core samples. Sowers and Jubenville (2000), Bock et al. (2010a) and Sapart et al. (2011) calibrated their system by introducing air standard gases over artificial, bubble-free ice (BFI) into the extraction unit to run a BFI analysis like an unknown ice core sample. We produced BFI from ultra-pure water. The water was degassed for over an hour by evacuation with a rotary pump while being stirred with a magnet bar and gently heated. Then the water was slowly frozen under vacuum from the bottom up by lifting a heated cover. The slow freezing process expelled most of the remaining gas molecules. Visible air inclusions were cut out of the BFI during sample preparation.

Our analytical setup was calibrated by a total of 35 air standard extractions over 8 BFI samples. The first air standard was injected over the frozen BFI sample in the evacuated melt-vessel. The BFI was then melted completely before the extraction was started. After the first extraction, the melted BFI sample was kept in the melt-vessel under vacuum. Air standards were then injected over the melted BFI sample and extracted after an equilibration time of 2 min. The air standards were taken from 4 different air mixtures (GIS, AL, NEEM, NOAA, history described in detail in Table 1), each with known isotopic composition and different mixing ratios of CH_4 and N_2O, respectively. By analyzing between 20 and 70 mL of the air standards, the calibration experiments covered a large range of sample sizes, including the amount of sample air to be expected from the extraction of 200–500 g of glacial and interglacial ice core samples (Fig. 6).

Two BFI samples that were produced in the same BFI batch contained dissolved gasses that only affected their first BFI measurement that included their melt process. This observation is in line with the description of Bock et al. (2010a) who found dissolved gases in BFI samples even though the BFI contained no visible gas inclusions. The stability of the consecutive extractions over melted BFI showed that a melted sample was completely degassed by the previous air-extraction. Changing the air standards of two consecutive injections showed no memory effect in the isotope ratios of CH_4 or N_2O, highlighting quantitative extraction. A significantly increased variability in both N_2O isotope ratios occurred during two days of BFI measurements. The data of these measurements were excluded, resulting in less N_2O data of BFI measurements as compared to CH_4 (Fig. 6). We speculate this effect is based on disequillibration effects inside the Hayesep in trap T2 after longer stand-by times. Regular use of T2 or pre-conditioning with adsorption-desorption cycles in case T2 hasn't been used for a while stabilized the N_2O isotope ratios. However, CH_4 measurements were unaffected. The system returned to stable analysis the following day.

The isotope ratio of the BFI measurements was referenced via isotope reference gas injections of 40 mL (GIS) to the respective international isotope scales. The linear regression of the isotope ratio offset versus the sample peak size was used to correct for differences in analyte amount of ice-core-air extractions from the melt-vessel and isotope reference gas extractions from T1 (Fig. 6). We found no significant isotope fractionation between the extractions from T1 and from the melt-vessel for experiments with identical amounts of analytes. We therefore conclude that there is no significant offset between the extraction of isotope reference gases from T1 and ice core samples from the melt-vessel. The occuring fractionation is therefore only based on the analyte amount. The correction according to the linear regression (Fig. 6) covers the necessary corrections that relate all samples to the isotope scales as defined by 40 mL of the isotope reference gas (described in Sect. 4). The sample-size corrected BFI measurements show a standard deviation (1σ) of 0.09 ‰ for $\delta^{13}C{-}CH_4$, 0.5 ‰ for $\delta^{15}N{-}N_2O$ and 0.7 ‰ for $\delta^{18}O{-}N_2O$.

4 Measurement correction and referencing protocol

The ice core measurement routine is shown in Table 2 and the routine for atmospheric gases from air tanks is shown in Table 3. Blocks of three GIS measurements preceded and succeeded the ice core sample and the quality control standard (QCS) measurements, respectively. For each isotope reference gas measurement, 40 mL of GIS were extracted from T1. The offset between the average isotope ratio determined for each block and the target isotope ratio assigned to GIS was considered to indicate the daily offset of the system to the international isotope scales, including the system drift between the beginning and the end the measurement day. The isotope ratio measurements of the ice core samples and the quality control standards were corrected for the sample size offset (Sect. 3.5) and then for the system offset as determined by GIS according to Werner and Brand (2001).

5 Results and discussion

5.1 Quality Control Standard measurements

One QCS measurement was included into each routine for ice core measurements (Table 2). The QCS were varied in size and evaluated as an unknown sample with corrections for size- and system variability (Sects. 3.5 and 4). The results of 17 QCS measurements for δ^{13}C–CH$_4$, δ^{15}N–N$_2$O and δ^{18}O–N$_2$O of the QCS from an ice core measurement campaign are plotted in the performance chart (Fig. 7). Since the BFI tests showed no detectable isotope fractionation between the BFI extractions from the melt-vessel and the reference gas extractions from T1, we consider the QCS extractions from T1 representative to indicate the magnitude of the measurement uncertainty that is inherent to the analysis of ice core samples. The standard deviation of the QCS measurements is therefore an important measure for the precision of the system. The estimated measurement uncertainty for δ^{13}C–CH$_4$ is 0.08 ‰ and 0.6 ‰ for both δ^{15}N–N$_2$O and δ^{18}O–N$_2$O, based on the 1σ standard deviation of the QCS measurements.

5.2 Reproducibility of ice core measurements

We measured 15 ice core samples (200–500 g) from the EUROCORE and NEEM ice core (gas age 657–1766 AD) to compare the performance of the setup with published δ^{13}C–CH$_4$ data (Fig. 8). 11 of these samples are measured as replicates that are divided in 5 groups of 2–3 samples with a maximum age difference within each group of less than 14 yr. We assume these grouped samples to contain air of similar composition and calculate the pooled standard deviation for δ^{13}C–CH$_4$ in these 11 samples of 0.07 ‰, representing a measure for the reproducibility of the measurements. Unfortunately we cannot provide the according N$_2$O data of these samples as the measurement routine for N$_2$O measurements was not fully developed at the time these ice core measurements were done.

5.3 Precision of the setup

Multiple gases which differ in the isotopic composition as well as in the mixing ratio of CH$_4$ and N$_2$O were injected over BFI to calibrate the system. One measurement of AL in variable amounts was included as QCS measurement during every day of ice core measurements to monitor the performance of the analytical setup including the data processing. Finally, we showed the reproducibility for the δ^{13}C–CH$_4$ measurements of the setup by the pooled standard deviation of 11 pre-industrial ice core samples between 200 and 500 g. We find the uncertainty estimate based on the analysis of ice core samples most representative on the one hand but it is restricted on the other hand because each ice core sample represents a unique air mixture that may be affected by atmospheric variability and the stochastic nature of bubble trapping. Even two adjacent ice core samples are therefore not necessarily 100 % identical. This problem of system calibration can be circumvented by repeated analysis of isotope reference gases from pressurized tanks. For the δ^{13}C–CH$_4$ measurement, the uncertainty estimates as derived from the BFI measurements, the QCS measurements and the pooled standard deviation of ice core sample measurements are in good agreement, suggesting that a realistic measurement uncertainty is estimated by all 3 methods. For the isotopic analysis of N_2O, the uncertainty estimate of the BFI and the QCS measurements also agree well. Based on the good match of the uncertainty estimates discussed for δ^{13}C–CH_4, we suggest that the uncertainty of N_2O measurements can reliably be estimated from the BFI and QCS measurements. For all measured parameters, we chose to state the uncertainty with the highest value, independent of the method from which it was derived. We therefore conclude a measurement uncertainty of 0.09 ‰ for δ^{13}C–CH_4 (BFI), 0.6 ‰ for δ^{15}N–N_2O (QCS) and 0.7 ‰ for δ^{18}O–N_2O (BFI), which is comparable to or better than Sowers et al. (2003), Ferretti et al. (2005), Schaefer and Whiticar (2007), Behrens et al. (2008), Sowers (2009), Sapart et al. (2011) and Melton et al. (2011).

5.4 Comparison to published ice core data and established systems

5.4.1 δ^{13}C–CH_4

We measured a total of 15 EUROCORE and NEEM ice core samples for δ^{13}C–CH_4 and compared our results with NEEM ice core data that were recently published by Sapart et al. (2012b) as shown in Fig. 8. Our data and the data from Sapart et al. (2012b) will be referred to as CIC and IMAU, respectively. For the data comparison, the IMAU data were corrected for the Kr-effect which was not known at the time of publication. We selected 6 data points of the IMAU dataset between 677 and 1757 AD and measured between 1 and 4 samples per IMAU data point on our setup. The gas age difference between the CIC and the respective IMAU samples ranged between 1 and 24 yr.

CIC and IMAU data show excellent agreement during 5 time intervals that cover a δ^{13}C–CH_4 range of nearly 2 ‰ (Fig. 8). However, we found a disagreement of ~ 1 ‰ in 4 CIC samples during the δ^{13}C–CH_4 excursion reported by Sapart et al. (2012b) at 964 AD. Since we can safely exclude Kr interferences as reason for the offset in both the CIC and the IMAU data, we assume that the differences between CIC and IMAU are likely due to differences in the sample preparation and the ice extraction technique.

While exceptionally thick layers of particles in the ice core samples were removed during sample preparation at CIC, some small gravel in the middle of the sample showing the disagreement was not removed at IMAU. Because it is not yet clear whether, and how particles could possibly cause artefacts in δ^{13}C$-$CH$_4$ measurements, the link between particles and isotope offset remains unclear. However, Rhodes et al. (manuscript in review) describe a correlation of particle enclosures in ice core samples and CH$_4$ mixing ratio anomalies, thereby supporting our hypothesis. Another analytical difference between CIC and IMAU is the technique to extract air from ice core samples. While a continuous melt-extraction technique is used at CIC, IMAU facilitates a dry-extraction technique (Sapart et al., 2011). Both techniques are tested and optimized for high extraction efficiency and both techniques delivered very similar results; it can therefore be excluded that conceptual differences of the extraction techniques alone caused the observed disagreement in δ^{13}C$-$CH$_4$ during one particular time interval. Even though visible particle layers were removed from the CIC samples, it can be expected that small particles were not removed. For the time being, we can only hypothesize that particles may have caused δ^{13}C$-$CH$_4$ artefacts when in contact with water during the melt-extraction of CIC or when hitting stainless-steel surfaces of the dry-extraction system of IMAU. Systematic studies on the formation of δ^{13}C$-$CH$_4$ artefacts in ice core samples with extraordinary particle layers would be required to further investigate this problem. However, this exceeds the scope of this study but represents an important field for future research. Based on the coincidence of particles and δ^{13}C$-$CH$_4$ offset, we assume that a high content of particles, possibly in combination with either wet- or dry-extraction technique has caused the δ^{13}C$-$CH$_4$ artefacts.

Because the data comparison between CIC and IMAU shows excellent agreement during all other time intervals, we find our setup suitable for δ^{13}C$-$CH$_4$ measurements in ice core samples. A δ^{13}C$-$CH$_4$ record of firn air samples was measured on our setup and also shows very good agreement with the results from other systems as published by Sapart et al. (2012a).

5.4.2 $\delta^{15}N-N_2O$ and $\delta^{18}O-N_2O$

A flask intercomparison study for N_2O isotope ratios in 3 different gas mixtures were conducted to compare our setup to the setup described by Sapart et al. (2011). The air mixtures used for this test varied by ~ 7 and ~ 6 ‰ in $\delta^{15}N$ and $\delta^{18}O$, respectively (Table 1). The results for all gases showed excellent agreement within the uncertainty of the measurements and were published earlier (Sapart et al., 2011).

So far, intercomparison measurements on isotope ratios of N_2O in ice core samples have not been made in the ice core community, and data for the time period of our $\delta^{13}C-CH_4$ comparison measurements (657–1766 AD) are lacking. We can therefore not give an ice core intercomparison at this stage but emphasize the need for the future.

6 Conclusions

We described our setup to measure $\delta^{13}C-CH_4$, $\delta^{15}N-N_2O$ and $\delta^{18}O-N_2O$ isotope ratios in air- and ice core samples and thoroughly discussed its performance and measurement uncertainty based on bubble free ice and quality control standard measurements. We proved the reproducibility of the analytical system and the suggested data processing method based on detailed experiments with sample amounts that can be expected in 200–500 g of glacial and interglacial ice core samples. We furthermore compared our ice core measurement for $\delta^{13}C-CH_4$ with published data which prove that our setup is capable of highlighting small yet significant isotope variations with excellent precision. A previously published intercomparison of isotope measurements of N_2O in isotope reference gases proved the described setup in very good agreement with established systems. A high resolution dataset of $\delta^{15}N-N_2O$ and $\delta^{18}O-N_2O$ measurements from ice core samples between 657 and 1766 AD is not available for intercomparison. However, we discussed measurements control strategies analogue to our δ^{13}C–CH$_4$ measurements that suggest our setup is suitable to reliably measure the isotopic composition of N$_2$O in ice core samples. We conclude that the precision of our setup for δ^{13}C–CH$_4$, δ^{15}N–N$_2$O and δ^{18}O–N$_2$O measurements is 0.09, 0.6 and 0.7 ‰, respectively. Especially the excellent precision of δ^{13}C–CH$_4$ of our setup and its independence of Kr interference make our setup suitable to analyze the variability of the interhemispheric gradient of CH$_4$ and of small changes of δ^{13}C–CH$_4$ in high temporal resolution. Future work should also include the harmonization of similar analytical systems and sample preparation protocols to minimize measurement offsets.

Acknowledgements. We would like to thank the field teams that took the EUROCORE and NEEM samples. NEEM is directed and organized by the Center of Ice and Climate at the Niels Bohr Institute and US NSF, Office of Polar Programs. It is supported by funding agencies and institutions in Belgium (FNRS-CFB and FWO), Canada (NRCan/GSC), China (CAS), Denmark (FIST), France (IPEV, CNRS/INSU, CEA and ANR), Germany (AWI), Iceland (RannIs), Japan (NIPR), Korea (KOPRI), The Netherlands (NWO/ALW), Sweden (VR), Switzerland (SNF), UK (NERC) and the USA (US NSF, Office of Polar Programs). We greatly appreciated helpful discussions with Hinrich Schaefer, Katja Riedel, Peter Franz and Gordon Brailsford from NIWA and with Willi Brand from the MPI-BGC. We thank Michael Bock and Jochen Schmitt from Bern for discussions and intercomparison measurements and we are greatful for the support of Colleen Templeton.

References

Anicich, V. G.: Evaluated bimolecular ion-molecule gas-phase kinetics of positive-ions for use in modeling planetary-atmospheres, cometary comae, and interstellar clouds, J. Phys. Chem. Ref. Data, 22, 1469–1569, 1993.

Aoki, N. and Makide, Y.: The concentration of krypton in the atmosphere – its revision after half a century, Chem. Lett., 34, 1396–1397, doi:10.1246/cl.2005.1396, 2005.

Behrens, M., Schmitt, J., Richter, K. U., Bock, M., Richter, U. C., Levin, I., and Fischer, H.: A gas chromatography/combustion/isotope ratio mass spectrometry system for high-precision δ^{13}C measurements of atmospheric methane extracted from ice core samples, Rapid Commun. Mass Sp., 22, 3261–3269, doi:10.1002/rcm.3720, 2008.

Bock, M., Schmitt, J., Behrens, M., Möller, L., Schneider, R., Sapart, C., and Fischer, H.: A gas chromatography/pyrolysis/isotope ratio mass spectrometry system for high-precision δD measurements of atmospheric methane extracted from ice cores, Rapid Commun. Mass Sp., 24, 621–633, doi:10.1002/rcm.4429, 2010a.

Bock, M., Schmitt, J., Möller, L., Spahni, R., Blunier, T., and Fischer, H.: Hydrogen isotopes preclude marine hydrate CH_4 emissions at the onset of Dansgaard-Oeschger events, Science, 328, 1686–1689, doi:10.1126/science.1187651, 2010b.

Brand, W. A.: Precon: a fully automated interface for the pre-GC concentration of trace gases in air for isotopic analysis, Isot. Environ. Healt. S., 31, 277–284, doi:10.1080/10256019508036271, 1995.

Brand, W. A.: Mass spectrometer hardware for analyzing stable isotope ratios, in: Handbook of Stable Isotope Analytical Techniques, Vol. 1, edited by: Groot, P. A., Elsevier B. V., Amsterdam, 835–856, 2004.

Brenninkmeijer, C. A. M.: Measurement of the abundance of ^{14}CO in the atmosphere and the ^{13}C/^{12}C and ^{18}O/^{16}O ratio of atmospheric CO with applications in New-Zealand and Antarctica, J. Geophys. Res.-Atmos., 98, 10595–10614, doi:10.1029/93jd00587, 1993.

Brenninkmeijer, C. A. M., Janssen, C., Kaiser, J., Rockmann, T., Rhee, T. S., and Assonov, S. S.: Isotope effects in the chemistry of atmospheric trace compounds, Chem. Rev., 103, 5125–5161, doi:10.1021/cr020644k, 2003.

Carter, J. F. and Barwick, V. J.: Good Practice Guide for Isotope Ratio Mass Spectrometry, 1st Edn., 1–48, ISBN 978-0-948926-31-0, 2011.

Cullis, C. F. and Willatt, B. M.: Oxidation of methane over supported precious metal-catalysts, J. Catal., 83, 267–285, doi:10.1016/0021-9517(83)90054-4, 1983.

Date, M., Ichihashi, Y., Yamashita, T., Chiorino, A., Boccuzzi, F., and Haruta, A.: Performance of Au/TiO_2 catalyst under ambient conditions, Catal. Today, 72, 89–94, doi:10.1016/s0920-5861(01)00481-3, 2002.

DesMarais, D. J.: Variable-temperature cryogenic trap for separation of gas-mixtures, Anal. Chem., 50, 1405–1406, doi:10.1021/ac50031a056, 1978.

Ferretti, D. F., Miller, J. B., White, J. W. C., Etheridge, D. M., Lassey, K. R., Lowe, D. C., Meure, C. M. M., Dreier, M. F., Trudinger, C. M., van Ommen, T. D., and Langenfelds, R. L.:

Unexpected changes to the global methane budget over the past 2000 years, Science, 309, 1714–1717, doi:10.1126/science.1115193, 2005.

Fischer, H., Behrens, M., Bock, M., Richter, U., Schmitt, J., Loulergue, L., Chappellaz, J., Spahni, R., Blunier, T., Leuenberger, M., and Stocker, T. F.: Changing boreal methane sources and constant biomass burning during the last termination, Nature, 452, 864–867, doi:10.1038/nature06825, 2008.

Flückiger, J., Blunier, T., Stauffer, B., Chappellaz, J., Spahni, R., Kawamura, K., Schwander, J., Stocker, T. F., and DahlJensen, D.: N_2O and CH_4 variations during the last glacial epoch: insight into global processes, Global Biogeochem. Cy., 18, GB1020, doi:10.1029/2003GB002122, 2004.

Friedli, H. and Siegenthaler, U.: Influence of N_2O on isotope analyses in CO_2 and mass-spectrometric determination of N_2O in air samples, Tellus B, 40, 129–133, 1988.

Ghosh, P. and Brand, W. A.: The effect of N_2O on the isotopic composition of air-CO_2 samples, Rapid Commun. Mass Sp., 18, 1830–1838, doi:10.1002/rcm.1560, 2004.

Kato, S., Akimoto, H., Braunlich, M., Röckmann, T., and Brenninkmeijer, C. A. M.: Measurements of stable carbon and oxygen isotopic compositions of CO in automobile exhausts and ambient air from semi-urban Mainz, Germany, Geochem. J., 33, 73–77, 1999.

Loulergue, L., Schilt, A., Spahni, R., Masson-Delmotte, V., Blunier, T., Lemieux, B., Barnola, J. M., Raynaud, D., Stocker, T. F., and Chappellaz, J.: Orbital and millennial-scale features of atmospheric CH_4 over the past 800 000 years, Nature, 453, 383–386, doi:10.1038/nature06950, 2008.

McPherson, J., Thompson, D., Pattrick, G., Holliday, R., Ramdayal, D., Khumalo, T., and Van der Lingen, E.: Commercial opportunities for gold catalysts, in: World Gold Conference 2009, Johannesburg, South Africa, 2009.

Melton, J. R., Whiticar, M. J., and Eby, P.: Stable carbon isotope ratio analyses on trace methane from ice samples, Chem. Geol., 288, 88–96, doi:10.1016/j.chemgeo.2011.03.003, 2011.

Melton, J. R., Schaefer, H., and Whiticar, M. J.: Enrichment in ^{13}C of atmospheric CH_4 during the Younger Dryas termination, Clim. Past, 8, 1177–1197, doi:10.5194/cp-8-1177-2012, 2012.

Merritt, D. A., Brand, W. A., and Hayes, J. M.: Isotope-ratio-monitoring gas-chromatography mass-spectrometry – methods for isotopic calibration, Org. Geochem., 21, 573–583, 1994.

Merritt, D. A., Freeman, K. H., Ricci, M. P., Studley, S. A., and Hayes, J. M.: Performance and optimization of a combustion interface for isotope ratio monitoring gas-chromatography mass-spectrometry, Anal. Chem., 67, 2461–2473, 1995.

Mitchell, L. E., Brook, E. J., Sowers, T., McConnell, J. R., and Taylor, K.: Multidecadal variability of atmospheric methane, 1000–1800 ce, J. Geophys. Res.-Biogeo., 116, G02007, doi:10.1029/2010jg001441, 2011.

Röckmann, T. and Levin, I.: High-precision determination of the changing isotopic composition of atmospheric N_2O from 1990 to 2002, J. Geophys. Res.-Atmos., 110, D2130410, doi:10.1029/2005jd006066, 2005.

Röckmann, T., Kaiser, J., Brenninkmeijer, C. A. M., and Brand, W. A.: Gas chromatography/isotope-ratio mass spectrometry method for high-precision position-dependent ^{15}N and ^{18}O measurements of atmospheric nitrous oxide, Rapid Commun. Mass Sp., 17, 1897–1908, doi:10.1002/rcm.1132, 2003.

Sapart, C. J., van der Veen, C., Vigano, I., Brass, M., van de Wal, R. S. W., Bock, M., Fischer, H., Sowers, T., Buizert, C., Sperlich, P., Blunier, T., Behrens, M., Schmitt, J., Seth, B., and Röckmann, T.: Simultaneous stable isotope analysis of methane and nitrous oxide on ice core samples, Atmos. Meas. Tech., 4, 2607–2618, doi:10.5194/amt-4-2607-2011, 2011.

Sapart, C. J., Martinerie, P., Chappellaz, J., van de Wal, R. S. W., Sperlich, P., van der Veen, C., Bernard, S., Sturges, W. T., Blunier, T., Witrant, E., Schwander, J., Etheridge, D., and Röckmann, T.: Reconstruction of the carbon isotopic composition of methane over the last 50 yr based on firn air measurements at 11 polar sites, Atmos. Chem. Phys. Discuss., 12, 9587–9619, doi:10.5194/acpd-12-9587-2012, 2012a.

Sapart, C. J., Monteil, G., Prokopiou, M., van de Wal, R. S. W., Kaplan, J. O., Sperlich, P., Krumhardt, K. M., van der Veen, C., Houweling, S., Krol, M. C., Blunier, T., Sowers, T., Martinerie, P., Witrant, E., Dahl-Jensen, D., and Röckmann, T.: Natural and anthropogenic variations in methane sources during the past two millennia, Nature, 490, 85–88, doi:10.1038/nature11461, 2012b.

Schaefer, H. and Whiticar, M. J.: Measurement of stable carbon isotope ratios of methane in ice samples, Org. Geochem., 38, 216–226, doi:10.1016/j.orggeochem.2006.10.006, 2007.

Schaefer, H., Whiticar, M. J., Brook, E. J., Petrenko, V. V., Ferretti, D. F., and Severinghaus, J. P.: Ice record of δ^{13}C for atmospheric CH_4 across the younger dryas-preboreal transition, Science, 313, 1109–1112, doi:10.1126/science.1126562, 2006.

Schilt, A., Baumgartner, M., Schwander, J., Buiron, D., Capron, E., Chappellaz, J., Loulergue, L., Schupbach, S., Spahni, R., Fischer, H., and Stocker, T. F.: Atmospheric nitrous oxide during the last 140 000 years, Earth Planet. Sc. Lett., 300, 33–43, doi:10.1016/j.epsl.2010.09.027, 2010.

Schmitt, J., Seth, B., Bock, M., van der Veen, C., Möller, L., Sapart, C. J., Prokopiou, M., Sowers, T., Röckmann, T., and Fischer, H.: On the interference of $^{86}Kr^{2+}$ during carbon isotope analysis of atmospheric methane using continuous flow combustion – isotope ratio mass spectrometry, Atmos. Meas. Tech. Discuss., 6, 1409–1460, doi:10.5194/amtd-6-1409-2013, 2013.

Sessions, A. L.: Isotope-ratio detection for gas chromatography, J. Sep. Sci., 29, 1946–1961, doi:10.1002/jssc.200600002, 2006.

Solomon, S., Qin, D., Manning, M., Alley, R. B., Berntsen, T., Bindoff, N. L., Chen, Z., Chidthaisong, A., Gregory, J. M., Hegerl, G. C., Heimann, M., Hewitson, B., Hoskins, B. J., Joos, F., Jouzel, J., Kattsov, V., Lohmann, U., Matsuno, T., Molina, M. J., Nicholls, N., Overpeck, J., Raga, G., Ramaswamy, V., Ren, J., Rusticucci, M., Somerville, R., Stocker, T. F., Whetton, P., Wood, R. A., and Wratt, D.: Climate change 2007: The physical science basis, Contribution of working group i to the fourth assessment report of the intergovernmental panel on climate change, 2007.

Sowers, T.: Late quaternary atmospheric CH_4 isotope record suggests marine clathrates are stable, Science, 311, 838–840, doi:10.1126/science.1121235, 2006.

Sowers, T.: Atmospheric methane isotope records covering the holocene period, Quaternary Sci. Rev., 29, 213–221, doi:10.1016/j.quascirev.2009.05.023, 2009.

Sowers, T. and Jubenville, J.: A modified extraction technique for liberating occluded gases from ice cores, J. Geophys. Res.-Atmos., 105, 29155–29164, 2000.

Sowers, T., Alley, R. B., and Jubenville, J.: Ice core records of atmospheric N_2O covering the last 106 000 years, Science, 301, 945–948, 2003.

Sowers, T., Bernard, S., Aballain, O., Chappellaz, J., Barnola, J. M., and Marik, T.: Records of the $\delta^{13}C$ of atmospheric CH_4 over the last 2 centuries as recorded in antarctic snow and ice, Global Biogeochem. Cy., 19, GB2002, doi:10.1029/2004GB002408, 2005.

Sperlich, P., Guillevic, M., Buizert, C., Jenk, T. M., Sapart, C. J., Schaefer, H., Popp, T. J., and Blunier, T.: A combustion setup to precisely reference $\delta^{13}C$ and $\delta^{2}H$ isotope ratios of pure CH_4 to produce isotope reference gases of $\delta^{13}C-CH_4$ in synthetic air, Atmos. Meas. Tech., 5, 2227–2236, doi:10.5194/amt-5-2227-2012, 2012.

Stowasser, C., Buizert, C., Gkinis, V., Chappellaz, J., Schüpbach, S., Bigler, M., Faïn, X., Sperlich, P., Baumgartner, M., Schilt, A., and Blunier, T.: Continuous measurements of methane mixing ratios from ice cores, Atmos. Meas. Tech., 5, 999–1013, doi:10.5194/amt-5-999-2012, 2012.

Sturm, P., Leuenberger, M., Sirignano, C., Neubert, R. E. M., Meijer, H. A. J., Langenfelds, R., Brand, W. A., and Tohjima, Y.: Permeation of atmospheric gases through polymer o-rings used in flasks for air sampling, J. Geophys. Res.-Atmos., 109, D0430910, doi:10.1029/2003JD004073, 2004.

Umezawa, T., Aoki, S., Nakazawa, T., and Morimoto, S.: A high-precision measurement system for carbon and hydrogen isotopic ratios of atmospheric methane and its application to air samples collected in the western pacific region, J. Meteorol. Soc. Jpn., 87, 365–379, doi:10.2151/jmsj.87.365, 2009.

Vaughn, B. H., Miller, J., Ferretti, D. F., and White, J. W. C.: Stable isotope measurements of atmospheric CO_2 and CH_4, in: Handbook of Stable Isotope Analytical Techniques, edited by: Groot, P. A., Elsevier B. V., Amsterdam, 272–304, 2004.

Werner, R. A. and Brand, W. A.: Referencing strategies and techniques in stable isotope ratio analysis, Rapid Commun. Mass Sp., 15, 501–519, 2001.

Table 1. Applied gases. Isotope reference gas names are listed in column 1. Column 2, 3 and 4 inform on the calibration path for δ^{13}C−CH_4, the determined δ^{13}C and the mixing ratio of CH_4. The referencing path for N_2O is mentioned in column 5 while column 6, 7, and 8 indicate the δ^{15}N, the δ^{18}O and the mixing ratio of N_2O, respectively. The uncertainty estimates are based on the standard deviation (1σ) apart from [a], which is described by Sperlich et al. (2012). The [b] indicates when the referencing method of NEEM for the isotopic composition of N_2O is explained by Sapart et al. (2011). The standard deviation for the isotopic composition of N_2O in GIS is larger as compared to the other gases due to the calibration with two gases during measurements that were optimized to measure δ^{13}C−CH_4. The larger scatter results from the measurement of small N_2O amounts. Note that the mean value of the QCS measurements for the isotopic composition of N_2O proves very good accuracy for the calibration of GIS (Fig. 7).

Gas	referencing [CH_4]	δ^{13}C−CH_4 [‰]	[CH_4] [ppb]	referencing [N_2O]	δ^{15}N−N_2O [‰]	δ^{18}O−N_2O [‰]	[N_2O] [ppb]
GIS	RM-8563	−42.21 ± 0.04[a]	429	NEEM/AL	−1.05 ± 0.6	40.09 ± 0.5	345
NEEM	IMAU/Bern	−47.30 ± 0.01	1839	IMAU/[b]	6.49 ± 0.04	44.58 ± 0.06	322
AL	NEEM/GIS	−49.55 ± 0.16	716	IMAU/NEEM	1.01 ± 0.15	38.8 ± 0.4	272
NOAA	NEEM	−38.57 ± 0.05	1642	IMAU/NEEM	−0.46 ± 0.15	41.06 ± 0.4	332

Table 2. Measurement sequence for ice core samples. A sequence for 2 ice core sample measurements comprises of 11 extraction measurements. Column 2 describes the function of each extraction. Column 3 and 4 inform on name and amount of the extracted sample while column 5 specifies the way the samples are introduced and column 6 shows from which analytical component the respective sample is extracted.

extraction	function	name	amount	introduction	extracted from
1	isotope reference gas	GIS	40 mL	MFC	T1
2	isotope reference gas	GIS	40 mL	MFC	T1
3	isotope reference gas	GIS	40 mL	MFC	T1
4	ice core sample	ice	200–500 g	manual	melt-vessel
5	blank test	blank	–	–	melt-vessel
6	quality control standard	AL	30–50 mL	MFC	T1
7	ice core sample	ice	200–500 g	manual	melt-vessel
8	blank test	blank	–	–	melt-vessel
9	isotope reference gas	GIS	40 mL	MFC	T1
10	isotope reference gas	GIS	40 mL	MFC	T1
11	isotope reference gas	GIS	40 mL	MFC	T1

Table 3. Measurement sequence for air samples from flasks or tanks. The presented sequence is used for triplet measurements of two samples, bracketed by isotope reference gas triplets. Column 2 describes the function of the measured gas which is described and quantified in column 3 and 4, respectively. Column 5 indicates that all samples are injected through the mass flow controller (MFC), directly into T3 or to be extracted from T1, as indicated in column 6.

extraction	function	name	amount	introduction	extracted from
1	isotope reference gas	NEEM	40 mL	MFC	T1/T3
2	isotope reference gas	NEEM	40 mL	MFC	T1/T3
3	isotope reference gas	NEEM	40 mL	MFC	T1/T3
4	air sample 1	[. . .]	40 mL	MFC	T1/T3
5	air sample 1	[. . .]	40 mL	MFC	T1/T3
6	air sample 1	[. . .]	40 mL	MFC	T1/T3
7	isotope reference gas	NEEM	40 mL	MFC	T1/T3
8	isotope reference gas	NEEM	40 mL	MFC	T1/T3
9	isotope reference gas	NEEM	40 mL	MFC	T1/T3
10	air sample 2	[. . .]	40 mL	MFC	T1/T3
11	air sample 2	[. . .]	40 mL	MFC	T1/T3
12	air sample 2	[. . .]	40 mL	MFC	T1/T3
13	isotope reference gas	NEEM	40 mL	MFC	T1/T3
14	isotope reference gas	NEEM	40 mL	MFC	T1/T3
15	isotope reference gas	NEEM	40 mL	MFC	T1/T3

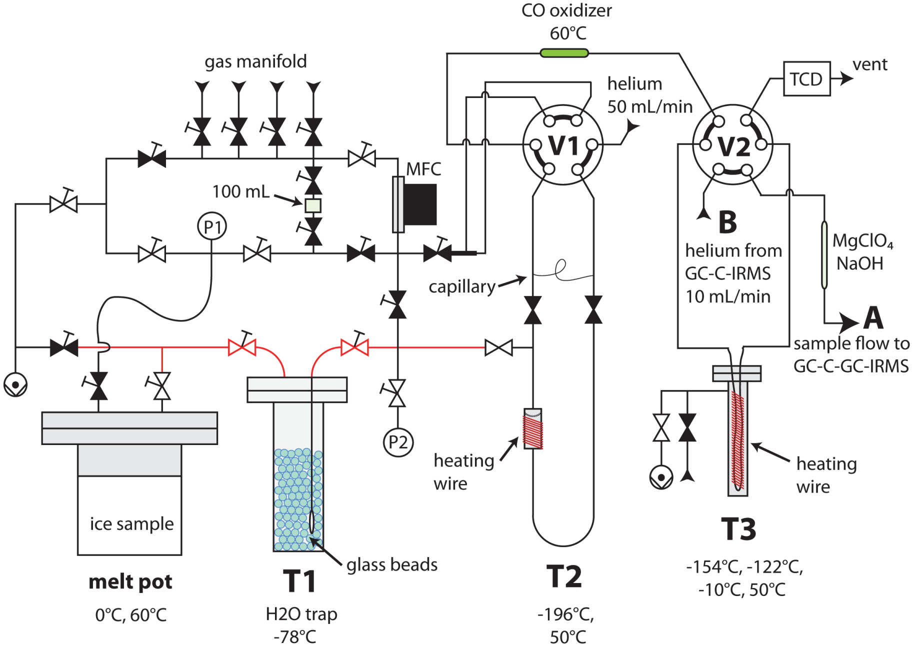

Fig. 1. Extraction unit design and flow scheme. Valve symbols with a handle symbolize manually operated valves while symbols without handle indicate automatically actuated valves. Filled valve symbol indicate closed valves, open symbols represent open valves. The figure shows the valve positioning of the extraction line during the melt-extraction of an ice core sample. The red lines mark the section of the extraction unit which is thermally insulated and heated to 55 °C. The letters A and B identify the ports of V2 that are connected to the respective port A at V5 and port B at V4 of the GC-C-GC-IRMS setup (Fig. 2). Port A transfers the sample to the GC-C-GC-IRMS unit while port B receives the carrier-gas flow for A.

Title Page
Abstract
Introduction
Conclusions
References
Tables
Figures
◀❙
❙▶
◀
▶
Back
Close
Full Screen / Esc
Printer-friendly Version
Interactive Discussion

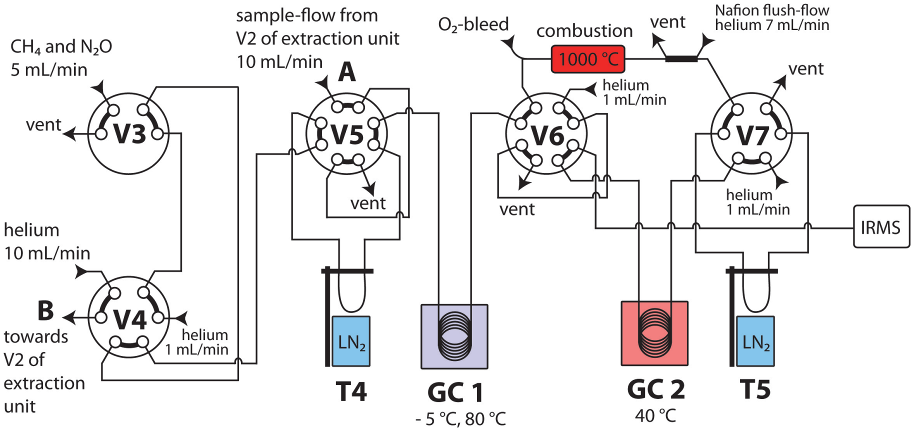

Fig. 2. Flow scheme of the GC-C-GC-IRMS unit. The letters A and B show the valve ports that connect to the ports A and B of the ice extraction unit, respectively. The CH_4 and N_2O sample is delivered to port A of the GC-C-GC-IRMS unit by the helium stream that flows out of the GC-C-GC-IRMS unit at port B.

Title Page
Abstract
Introduction
Conclusions
References
Tables
Figures
◀I
▶I
◀
▶
Back
Close
Full Screen / Esc
Printer-friendly Version
Interactive Discussion

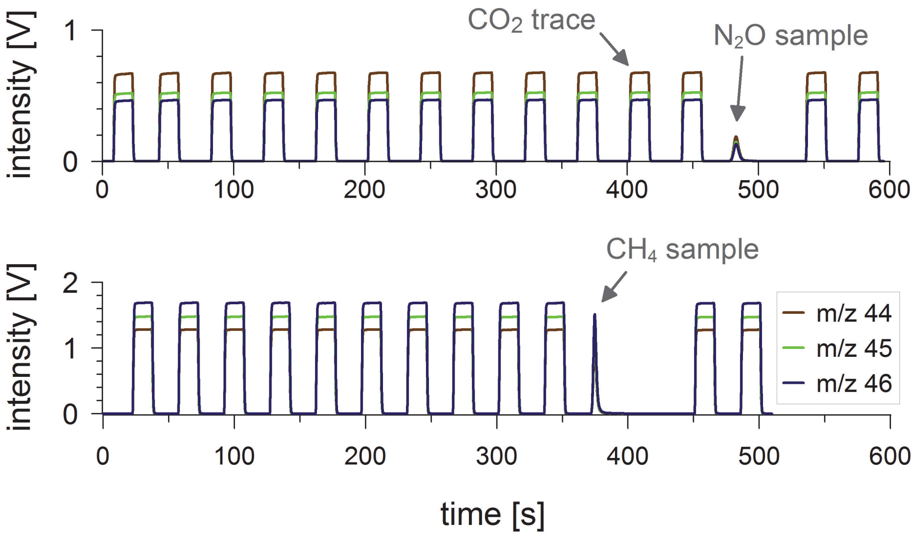

Fig. 3. Shown are the three traces *m/z* 44, 45 and 46 of two chromatograms for the determination of δ^{15}N$-$N$_2$O and δ^{18}O$-$N$_2$O (top panel) and for δ^{13}C$-$CH$_4$ (bottom panel). Reference gas peak 11 of the N$_2$O measurement includes the CO$_2$ remainder stemming from system blank and incomplete CO$_2$ removal by the Ascarite trap (Fig. 1). The chromatograms show the measurement of an ice core sample with low N$_2$O and CH$_4$ mixing ratios, typical for glacial periods.

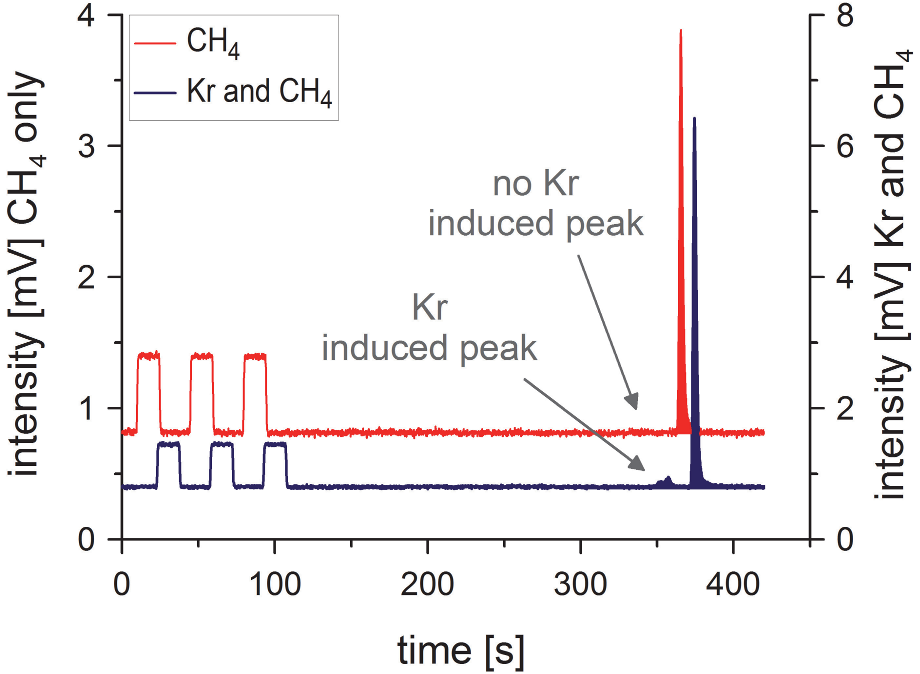

Fig. 4. The Krypton effect is visible when comparing the *m/z* 43 traces of $\delta^{13}C-CH_4$ measurements in an atmospheric air mixture (blue line, right axis) and in a pure CH_4 gas (red line, left axis), where the latter contains no Kr. Both peaks of CH_4-induced CO_2 occur on *m/z* 43 while the baseline separated peak induced by remnant Kr occurs only in the atmospheric sample. To avoid an overlap of the displayed peaks, the chromatogram of the pure CH_4 is shifted by 15 s.

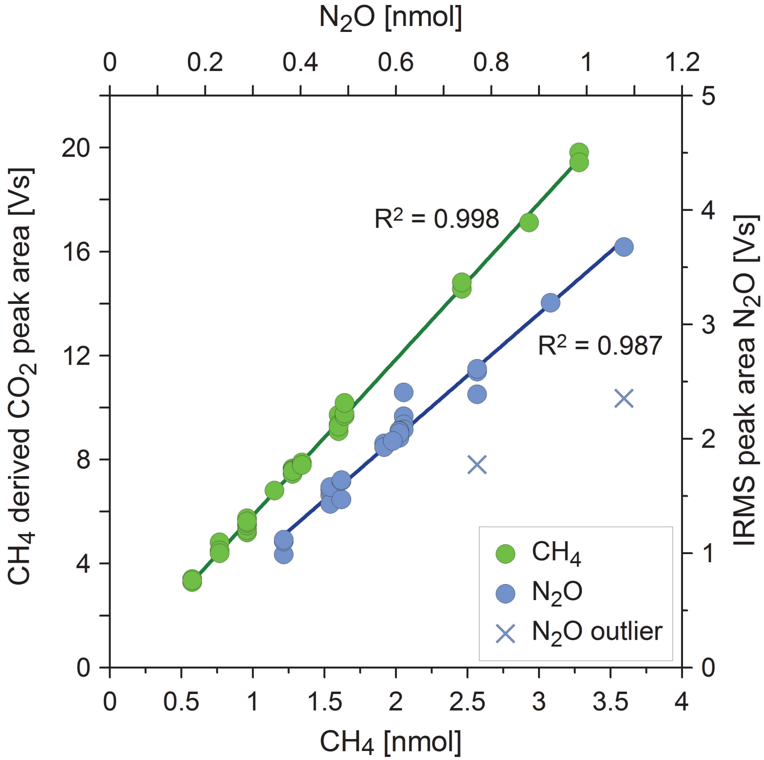

Fig. 5. Sample recovery. Green circles show the injected CH_4 amount [nmol] and the resulting IRMS peak area [Vs] as detected during bubble free ice measurements with the injection of 4 different air mixtures in variable amounts. Blue circles display analogue information for N_2O. The two blue crosses show outlier of N_2O that suffered from a loss of IRMS peak area for unknown reasons. Both outliers are therefore not included in the calculation of the regression.

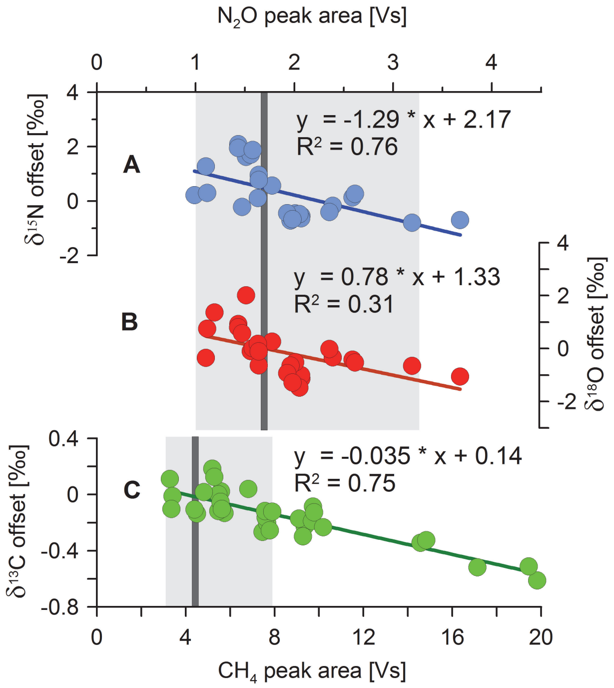

Fig. 6. Impact of sample size variability on the isotopic composition of δ^{15}N–N$_2$O **(A)**, δ^{18}O–N$_2$O **(B)** and δ^{13}C–CH$_4$ **(C)**. The offsets in isotopic composition of CH$_4$ and N$_2$O were determined in 33 and 26 BFI extractions, respectively. The dark grey lines indicate the IRMS peak area of the isotope reference gas measurements (GIS), which were used to reference the BFI samples to the respective isotope scales. The shaded zones indicate the IRMS peak area range of ice core sample measurements. Coloured lines display the linear regressions that are used to correct the isotopic composition of sample measurements for the difference in IRMS peak area between sample and isotope reference gas.

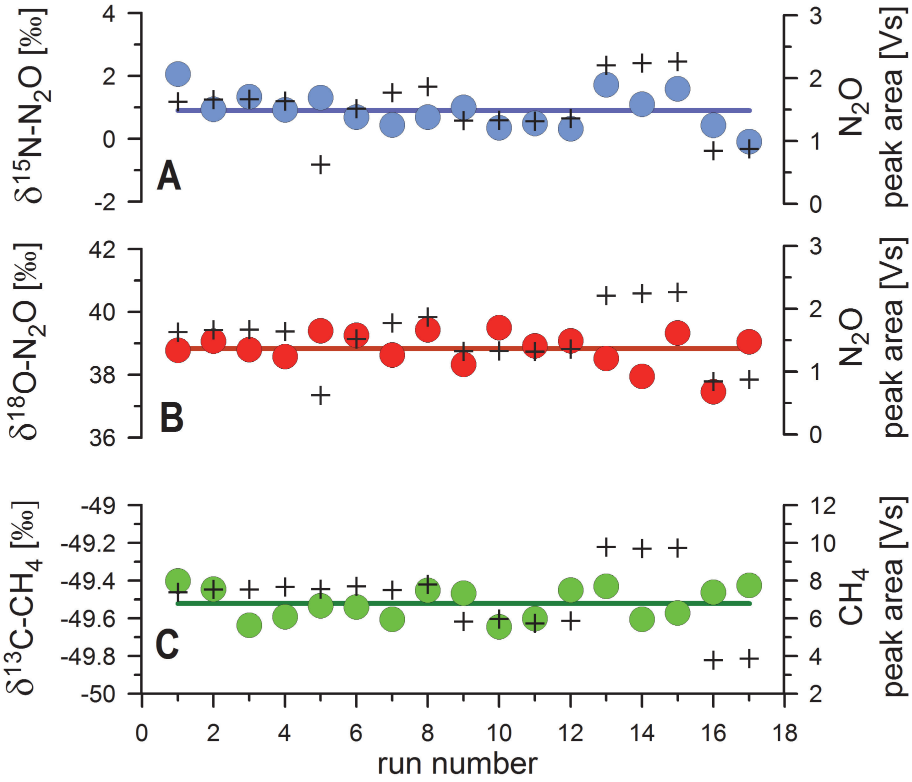

Fig. 7. Results of QCS measurements. The circles of the performance chart display the isotope ratio measurements of δ^{15}N−N$_2$O **(A)**, δ^{18}O−N$_2$O **(B)** and δ^{13}C−CH$_4$ **(C)** as determined during the QCS-measurements by injecting variable amounts of AL. The crosses relate to the y-axis on the right hand side and indicate the IRMS peak area of the respective measurement. The lines show the average δ values of the measurements.

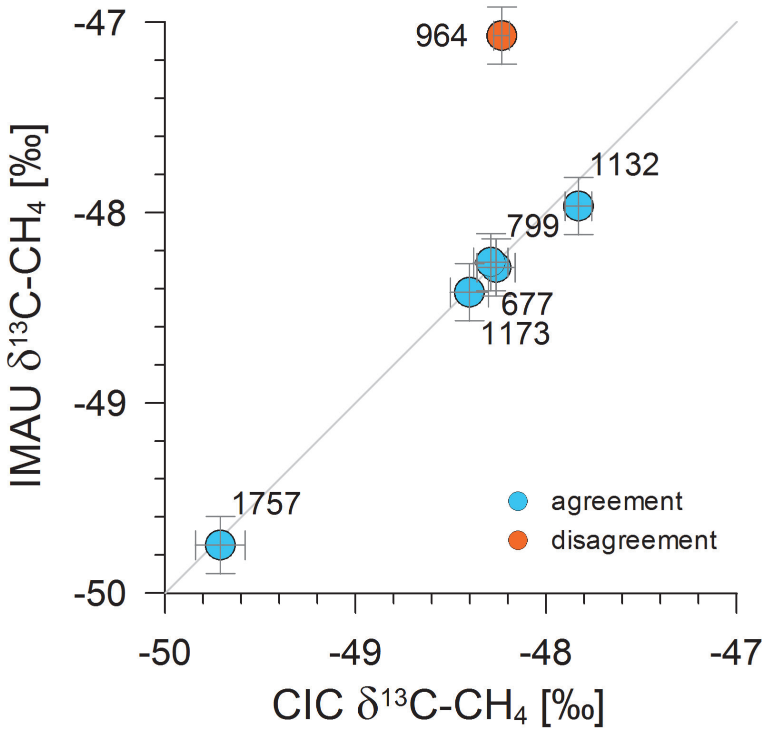

Fig. 8. Comparison of CIC and IMAU δ^{13}C$-$CH$_4$ ice core data. Blue circles indicate data comparison of time sections where good agreement was found. The orange circle indicates the period of time where CIC and IMAU found a disagreement of ∼1 ‰. Error bars indicate the measurement uncertainty or the average of the measurements used for the laboratory comparison. The labels display the time A.D. of the IMAU samples.